

Fe–Mg diffusion in olivine I: experimental determination between 700 and 1,200°C as a function of composition, crystal orientation and oxygen fugacity

Ralf Dohmen · Hans-Werner Becker ·
Sumit Chakraborty

Received: 4 October 2006 / Accepted: 19 March 2007 / Published online: 21 April 2007
© Springer-Verlag 2007

Abstract We have determined Fe–Mg diffusion coefficients in olivines from different sources (Nanga Parbat, Pakistan and San Carlos, Arizona, USA) at atmospheric pressure as a function of composition, oxygen fugacity (10^{-5} – 10^{-12} Pa) and temperature (700–1200°C) using thin films produced by pulsed laser deposition and RBS to analyze the concentration profiles. We have characterized the nano-scale structure and composition of the thin films annealed at various conditions and shown that the nature of the film (e.g. crystallinity, wetting behavior) depends strongly on the annealing conditions. If these variations are not taken into account in the form of boundary conditions for modeling the diffusion profiles, artifacts would result in the diffusion data. The diffusion coefficients obtained from 75 experiments reveal that (i) between fO_2 of 10^{-5} and 10^{-10} Pa, diffusion along all three principal crystallographic directions in olivine, [100], [010] and [001], are described by a constant activation energy of ~200 kJ/mol, precluding any temperature dependence of diffusion anisotropy and change of mechanism of diffusion at temperatures between 950 and 1200°C, (ii) diffusion coefficients increase with oxygen fugacity at $fO_2 > 10^{-10}$ Pa, with an fO_2 exponent that lies between 1/4 and 1/7, and (iii) at fO_2 below 10^{-10} Pa, and consequently at temperatures below ~900°C, diffusion becomes weakly dependent/independent of fO_2 , indicating a change of diffusion

mechanism. Activation energy of diffusion at these conditions is slightly *higher*, ~220 kJ/mol. The data, including the change of mechanism, are analyzed in terms of point defect chemistry in Part II of this work to derive an equation that allows calculation of diffusivities in olivine over its entire field of stability. Availability of directly measured data at temperatures down to 700°C imply that for the first time diffusion coefficients can be *interpolated*, rather than *extrapolated*, for modeling most natural systems.

Keywords Olivine · Diffusion · Point defects · Thin films · Nanostructure · Pulsed Laser Deposition · Rutherford Backscattering Spectroscopy · Mineral kinetics

Introduction

Diffusion of octahedrally coordinated cations in olivine, such as Fe, Mg, Ni, Mn and Ca, has been the focus of many experimental studies since the first measurements of Ni diffusion by Clark and Long (1971) (e.g. Buening and Buseck 1973; Misener 1974; Morioka 1981; Nakamura and Schmalzried 1984; Jurewicz and Watson 1988; Morioka and Nagasawa 1991; Chakraborty et al. 1994; Chakraborty 1997; Jaoul et al. 1995; Ito et al. 1999; Petry et al. 2004; Coogan et al. 2005; Hier-Majumder et al. 2005). This extensive interest arises from the wide range of applications of such data spanning fields such as cosmochemistry, igneous and metamorphic petrology, mantle geochemistry and mineral physics. The majority of studies cited above were concerned with the determination of diffusion rates of the major elements Fe and Mg in olivines. But in spite of this elaborate experimental effort a number of questions remain controversial or unanswered. For example, discrepancies exist between values of Fe–Mg exchange

R. Dohmen (✉) · S. Chakraborty
Institut für Geologie, Mineralogie und Geophysik,
Ruhr-Universität Bochum, 44780 Bochum, Germany
e-mail: ralf.dohmen@rub.de

H.-W. Becker
Institut für Physik mit Ionenstrahlen,
Ruhr-Universität Bochum, 44780 Bochum, Germany

diffusion coefficients measured by different authors (e.g. Buening and Buseck 1973; Misener 1974; Jurewicz and Watson 1988; Jaoul et al. 1995; Chakraborty 1997) and the dependence of Fe–Mg diffusion coefficients on important parameters such as composition and oxygen fugacity remain inadequately quantified. There are also questions regarding extrapolation of these diffusion coefficients to lower temperatures (<1,000°C) because available experimental data (Jaoul et al. 1995) appear to be inconsistent with extrapolations of high temperature data. We have utilized recent developments in thin film technology to carry out a detailed experimental study to address these issues. The purpose of this paper is to (1) present the method of determination of diffusion coefficients using thin films, with an emphasis on the aspects of deposition and characterization of thin silicate films that are essential for avoiding artifacts, (2) present diffusion coefficients measured in olivine as a function of temperature, composition and oxygen fugacity, and (3) discuss the discrepancies between various data-sets in the light of sample characterization, observations and data from the new experiments that were obtained using methods that have only recently become available. We demonstrate that most of the discrepancy is either apparent or attributable to specific features of earlier experimental work. In an accompanying paper (referred to henceforth as Part II) we analyze the data, taking into account the point defect chemistry of olivine as well as the impurities that are commonly present in natural olivine to understand the mechanism of diffusion. Finally, we combine the experimental data with this knowledge of diffusion mechanisms to derive a master equation for the calculation of Fe–Mg diffusion coefficients in olivine as a function of pressure, temperature, composition, oxygen fugacity and crystallographic orientation.

Any determination of diffusion coefficients at temperatures below 1,000°C requires the use of nano-scale techniques, because diffusion length scales are expected to be on the order of 100 nm for feasible experimental duration. We have used the new technique of Pulsed Laser Deposition (PLD) to produce well-defined diffusion couples on the nano-scale consisting of thin films (crystalline or amorphous) on a single crystal. Induced diffusion profiles have been measured using Rutherford Backscattering Spectroscopy (RBS). We have published two preliminary data points measured with this setup in Dohmen et al. (2002). In this paper, we report on a complete data set for Fe–Mg diffusion along the three principal crystallographic axes between 700 and 1,200°C. The dependence of this diffusion coefficient on fO_2 was determined at these temperatures over almost the entire stability field of olivine. The compositional dependence of the diffusion coefficient has been determined at temperatures $\leq 1,000^\circ\text{C}$.

Experimental methods

Preparation of diffusion couples and sample treatment

Single crystals of gem quality olivine from two locations (Nanga Parbat, Pakistan—O11 and San Carlos, Arizona, USA—O17, O15, O136, O140) were used for the diffusion experiments. Their compositions are provided in Table 1. These crystals were either oriented using X-ray Laue diffraction patterns (O11, O17, O15, O136) or optically with a spindle stage setup attached to a computer (O140). The oriented crystals were cut into slices (1–2 mm thickness) perpendicular to the [100], [010], or [001] axis (space group: Pbnm) and polished mechanically using diamond compounds with a final chemical–mechanical polishing step using colloidal silica compounds. The polished slices were finally cut using a precision diamond saw into pieces between 1 and 4 mm³ in size. The orientations of the polished surfaces have been verified from time to time using electron back-scatter diffraction in an SEM.

Diffusion couples consisting of thin films on these polished single crystals have been produced using the PLD (e.g. Chrisey and Hubler 1994 for a review). The principle of the method and the detailed experimental setup for the deposition have been published in Dohmen et al. (2002). As source material (target) for the deposition we have used polycrystalline synthesized olivine pellets with varying forsterite contents (Fo80, Fo70, Fo30, pure fayalite). The deposition conditions varied over some range for the different samples, a list of the detailed deposition conditions is given in Table 2. The most important difference between samples lies in the fact that two different wavelengths of the laser pulse (193 and 248 nm) have been used and that some samples were deposited at hot conditions (up to 620°C), which led to fractionation effects compared to the ideal composition (see below). In any case most of the samples were heated in vacuum (up to 620°C) before the deposition to degas volatile adsorbents on the polished surface.

Typically a batch of four to eight crystals were deposited simultaneously and from this set one crystal was used as a reference sample to measure the initial film thickness and composition (Table 2). Our calibrations have shown (Dohmen et al. 2002) that the variation in thickness of the deposited film over the whole area covered by the samples ($\sim 5 \times 5 \text{ mm}^2$) is less than 10%, and a variation in composition within this area has not been detected for any given deposition. We have produced various kinds of diffusion couples where the film compositions were chosen depending on the experimental temperature. The film thickness varied between 30 and 200 nm, where thinner films were chosen for the more fayalite-rich films. The optimum diffusion couples for a given temperature in the

Table 1 Microprobe data

	O11a	O11c	O11b	O17a1	O17b1	O17b2	O17c	O115c	O140/6c	O140/7c	O136c
WSiO ₂	41.03	41.90	40.83	41.28	41.13	41.67	40.85	41.09	40.80	40.84	40.82
WTiO ₂	0.01	0.00	0.02	0.02	0.01	0.02	0.00	0.01	0.02	0.03	0.01
wAl ₂ O ₃	0.04	0.02	0.03	0.03	0.03	0.03	0.04	0.05	0.04	0.05	0.03
wCr ₂ O ₃	0.04	0.02	0.02	0.03	0.03	0.03	0.03	0.05	0.02	0.03	0.02
WFeO	10.75	5.12	11.73	8.80	9.34	8.76	10.57	8.62	11.93	11.45	11.65
WMnO	0.16	0.18	0.17	0.13	0.13	0.11	0.15	0.11	0.17	0.17	0.17
WNiO	0.40	0.24	0.38	0.38	0.39	0.42	0.40	0.43	0.36	0.39	0.38
WMgO	48.43	52.95	47.65	49.67	49.21	50.44	48.22	49.80	47.90	47.80	47.46
WCaO	0.13	0.01	0.10	0.08	0.08	0.07	0.07	0.11	0.09	0.16	0.10
wTotOx	100.99	100.44	100.93	100.43	100.34	101.55	100.33	100.27	101.33	100.91	100.62
Si	1.0010	1.0010	1.0010	1.0032	1.0029	1.0011	1.0021	1.0000	0.9972	1.0004	1.0031
Al	0.0012	0.0004	0.0009	0.0009	0.0008	0.0009	0.0011	0.0014	0.0012	0.0014	0.0008
Cr	0.0007	0.0003	0.0004	0.0006	0.0006	0.0006	0.0006	0.0010	0.0005	0.0007	0.0003
Ti	0.0001	0.0000	0.0003	0.0003	0.0001	0.0003	0.0000	0.0001	0.0003	0.0005	0.0002
Fe	0.2192	0.1022	0.2404	0.1788	0.1906	0.1761	0.2169	0.1755	0.2440	0.2345	0.2394
Ni	0.0079	0.0046	0.0075	0.0075	0.0076	0.0082	0.0080	0.0084	0.0071	0.0077	0.0075
Mg	1.7610	1.8860	1.7413	1.7995	1.7889	1.8066	1.7634	1.8069	1.7456	1.7455	1.7387
Mn	0.0033	0.0037	0.0036	0.0027	0.0027	0.0022	0.0031	0.0023	0.0035	0.0034	0.0035
Ca	0.0035	0.0003	0.0027	0.0021	0.0021	0.0018	0.0019	0.0030	0.0023	0.0041	0.0027
SU1	1.9970	1.9975	1.9971	1.9924	1.9933	1.9967	1.9950	1.9986	2.0044	1.9978	1.9931
O	4	4	4	4	4	4	4	4	4	4	4
Fo	88.3	94.5	87.3	90.4	89.8	90.6	88.5	90.5	87.2	87.5	87.3
Fa	11.0	5.1	12.0	9.0	9.6	8.8	10.9	8.8	12.2	11.8	12.0
Cr ppm a.f.u.	736	304	370	645	591	645	594	982	483	653	340
Al ppm a.f.u.	1201	426	931	919	812	919	1091	1350	1208	1367	768

Where a.f.u denotes (number of atoms per formula unit of M₂SiO₄) × (10⁶)

sense of film thickness and composition has been established during the earlier stage of this study.

All diffusion anneals have been performed in a continuous flow CO + CO₂ gas mixing furnace at atmospheric pressure under controlled oxygen fugacity. Temperature and oxygen fugacity are monitored in situ by a type B thermocouple and a *f*O₂-sensor (stabilized zirconia from Ceramic Oxide Fabricators, Eaglehawk, Australia), respectively. The oxygen fugacity is controlled within an accuracy of ±0.1 log units, and temperature is accurate at least within ±2°C as calibrated with melting points of Ag, Au, Ni, and Pd. A selection of polished samples was pre-annealed before the deposition in the gas mixing furnace at 1,200 or 1,300°C under controlled oxygen fugacity within the stability field of olivine. The detailed list of run conditions for all samples are given in Table 3. Pre-annealing conditions are included in Table 2. After the diffusion anneal or pre-anneal the surface of the samples was analyzed qualitatively with a reflected light microscope and for a representative section of the samples the surface topography were analyzed quantitatively with a white light phase

shift interference microscope (IFM from ATOS, Darmstadt, Germany) in the phase mode. In addition some of the samples were investigated with a scanning electron microscope (SEM). All of the described methods were available at the Institut für Geologie, Mineralogie und Geophysik at the Ruhr Universität Bochum.

Rutherford Back Scattering Spectroscopy (RBS)

Rutherford Backscattering Spectroscopy (RBS) has been used to measure film thickness and composition of the reference samples as well as for the detailed analysis of the diffusion couples after the diffusion anneal including extraction of Fe concentration depth profiles. A description of the principles of RBS can be found in the monograph by Feldman (1986) and some examples of application of RBS for diffusion profile analysis in the Earth Sciences may be found in Cherniak et al. (1991) or Jaoul et al. (1991). Typically, the diffusion of a heavy trace element (e.g. rare earth) into a light matrix (e.g. silicate) is studied by RBS. So far there is only one study in which chemical diffusion

Table 2 List of deposition conditions and initial film composition

Substrates		Deposition conditions ^a					Thin film properties (RBS)			Preannealing conditions		
ID	Comp.	Target	ν (nm)	t (s)	T (°C)	P (Pa)	d (nm)	X_{Mg}	(Fe + Mg)/Si	T (°C)	T (h)	fO_2 (Pa)
[001]												
Ol1c1–4	Fo95	Fo80	248	300	530	5.0E-2	76	0.80	2.00			
Ol1c 5–8	Fo95	Fo80	248	300	530	5.0E-2	46	0.80	1.82			
Ol36c 5–8 ^b	Fo88	Fo80	248	360	530	5.0E-4	110	0.78	1.92	1270	3	1.0E-4
Ol15c25	Fo90	Fo80	248	240	20	1.0E-4	150	0.79	2.03			
Ol15c30–36 ^b	Fo90	Fo80	248	300	20	1.0E-4	140	0.79	2.03	1200	4	1.0E-7
Ol40/6c 1–4	Fo88	Fo80	193	600	20	4.0E-4	90	0.71	1.41			
Ol40/6c 5–7	Fo88	Fo80	193	900	20	8.0E-4	180	0.72	1.38			
Ol40/6c 8–11	Fo88	Fo80	193	900	20	8.0E-4	165	0.72	1.38			
Ol40/7c 1–6	Fo88	Fo30	193	600	620	2.0E-3	30	0.19	1.75			
Ol7c1–2	Fo90	Fo30	193	420	620	1.0E-4	70	0.20	1.81	1200	20	1.0E-7
Ol7c3–4	Fo90	Fo30	193	420	620	1.0E-4	70	0.20	1.81	1200	20	1.0E-2
Ol7c5–11	Fo90	Fo30	193	600	620	1.0E-4						
[100]												
Ol36a1–6	Fo90	Fo80	248	300	620	5.0E-2	108	0.81	2.00			
Ol1a15–18	Fo88	Fo80	248	360	20	5.0E-4	115	0.78	2.00			
Ol1a23–26	Fo88	Fo80	248	360	20	5.0E-4	100	0.78	2.00			
Ol7a2–5	Fo90	Fo80	193	420	20	1.5E-4	150	0.75	1.52	1200	3	1.0E-7
Ol7a12–13	Fo90	Fo80	248	240	20	1.0E-4	150	0.79	2.03			
Ol7a18–24	Fo90	Fo80	248	300	20	1.0E-4	150	0.78	2.04	1200	3	1.0E-7
Ol7a25–28	Fo90	Fo30	193	600	620	1.0E-3	45	0.35	1.70			
Ol7a29–38	Fo90	Fo80	193	600	20	1.0E-4	210	0.72	1.38			
Ol7a39–42	Fo90	Fo30	193	600	620	1.0E-3	50	0.35	1.70			
[010]												
Ol1b1–4	Fo89	Fo80	248	300	620	4.0E-2	83	0.80	2.00			
Ol1b5–8	Fo89	Fo80	248	300	20	4.0E-2	60	0.80	2.00			
Ol1b13–16	Fo89	Fo80	248	360	530	5.0E-2	150	0.79	1.91			
Ol1b17–20	Fo89	Fa100	248	360	100	1.0E-2	60	0.00	1.35	1270	2	1.0E-4
Ol1b21–23	Fo89	Fo80	248	600	400	3.0E-2	80	0.76	1.79			
Ol7b6–9	Fo91	Fo80	193	690	20	2.0E-2	140	0.75	1.61	1200	3	1.0E-7
Ol7b12	Fo91	Fo80	248	240	20	1.0E-4	150	0.79	2.03			
Ol7b17–23	Fo91	Fo80	248	300	20	1.0E-4	170	0.78	2.04	1200	2	1.0E-7
Ol7b24–30	Fo91	Fo30	193	600	620	1.0E-3	50	0.40	1.40			

The symbols have the following meaning: ν wave length of laser pulse, P total pressure in vacuum chamber, t time, T temperature, d film thickness. Bold numbers indicate depositions where the stoichiometry deviates significantly from the ideal olivine composition (silica excess)

^a Repetition rate: 10 Hz; laser fluence: 5–10 J/cm²

^b SiO₂ layer after pre-anneal

of Fe–Mg in a silicate–olivine—was studied by RBS (Jaoul et al. 1995). We published a preliminary data point for Fe–Mg diffusion in olivine using PLD thin films and RBS in Dohmen et al. (2002).

The RBS analyses have been carried out at the Dynamitron Tandem Accelerator Laboratory of the Ruhr-Universität Bochum. A 4 MeV Tandem accelerator is used to generate a beam of α -particles at 2 MeV, which are focused onto the sample. A final aperture of 0.5 mm diameter enables to analyze olivine samples with a surface

as small as 1 mm². For the measurements typically a beam current between 20 and 50 nA was used and to prevent charging of the samples a solution with Ag was painted on to the side of the samples to permit electrical contact with the metallic sample holder. The back-scattered particles are detected at an angle of 170° (160° for later samples) with a silicon particle detector at an energy resolution of about 16–20 keV. The sample surface was tilted at 5° relative to the beam direction to avoid channeling.

Table 3 List of annealed samples with run conditions and evaluated diffusion coefficients

Sample	<i>d</i> (nm)	<i>T</i> (°C)	<i>t</i> (min)	Log[<i>f</i> O ₂ (Pa)]	log[<i>D</i> (m ² /s)]
[100]					
OI36a1	90	900	4003	-10.0	-19.60
OI36a2	100	1000	1290	-10.0	-18.52
OI1a15	120	905	3920	-10.0	-19.70
OI1a24	110	850	1052	-10.0	-19.85
OI7a2	140	905	1057	-10.0	-19.30
OI7a3	140	851	4446	-10.0	-19.55
OI7a4	140	996	306	-7.0	-18.35
OI7a12	140	998	120	-7.0	-18.10
OI7a18	150	1200	30	-7.0	-17.10
OI7a19	150	1152	32	-7.0	-17.40
OI7a21	150	1052	71	-7.0	-18.00
OI7a22	150	1001	128	-7.0	-18.40
OI7a23	150	948	95	-7.0	-18.64
OI7a25	40	905	1541	-7.0	-19.03
OI7a26	40	905	115	-7.0	-18.89
OI7a27	40	905	208	-12.0	-19.34
OI7a29	180	1050	68	-5.0	-17.68
OI7a30	220	1050	62	-6.0	-17.82
OI7a31	210	1050	63	-7.0	-18.10
OI7a34	230	1050	75	-9.0	-18.46
OI7a35	220	1050	60	-10.0	-18.46
OI7a36	240	1050	60	-8.0	-18.09
OI7a37	210	1050	63	-10.0	-18.34
OI7a39	50	800	1260	-9.7	-20.10
OI7a41	40	900	120	-7.0	-18.80
[010]					
OI1b2	70	900	1080	-10.0	-19.64
OI1b3	90	1006	188	-10.0	-18.59
OI1b5	70	1006	1071	-10.0	-18.38
OI1b6	50	1006	56	-10.0	-18.70
OI1b7	50	1006	188	-7.0	-18.00
OI1b13	140	905	3920	-10.0	-19.33
OI1b21	80	798	3937	-10.0	-19.90
OI1b22	80	1000	271	-7.0	-18.30
OI1b17	60	903	323	-10.0	-19.05
OI1b18	60	798	354	-10.0	-19.96
OI7b6	120	905	1057	-10.0	-19.15
OI7b7	120	851	4446	-10.0	-19.52
OI7b8	120	996	306	-7.0	-18.30
OI7b12	140	998	120	-7.0	-18.10
OI7b17	150	1200	30	-7.0	-17.15
OI7b18	150	1152	32	-7.0	-17.40
OI7b20	140	1052	71	-7.0	-18.05
OI7b22	130	948	95	-7.0	-18.52
OI7b24	40	905	1541	-7.0	-18.96
OI7b25	40	905	115	-7.0	-18.82

Table 3 continued

Sample	<i>d</i> (nm)	<i>T</i> (°C)	<i>t</i> (min)	Log[<i>f</i> O ₂ (Pa)]	log[<i>D</i> (m ² /s)]
OI7b26	40	905	428	-7.0	-18.85
OI7b27	40	905	208	-12.0	-19.07
OI7b29	40	800	1260	-9.7	-20.10
[001]					
OI1c3	70	1006	188	-10.0	-18.66
OI1c5	50	1006	1071	-10.0	-18.72
OI1c6	50	1006	56	-10.0	-18.49
OI1c7	50	1006	188	-7.0	-18.17
OI36c6	120	1102	51	-7.0	-16.60
OI15c25	140	998	120	-7.0	-17.54
OI15c33	120	1052	71	-7.0	-17.10
OI40/6c 1	85	1080	25	-5.0	-16.19
OI40/6c 2	85	1080	28	-11.0	-17.37
OI40/6c 3	85	1080	25	-8.0	-16.89
OI40/6c 5	160	1080	25	-6.0	-16.77
OI40/6c 6	180	1080	25	-7.0	-16.72
OI40/6c 8	180	1080	25	-9.0	-17.42
OI40/6c 9	180	1080	25	-10.0	-17.47
OI40/7c1	40	905	1541	-7.0	-18.27
OI40/7c2	30	905	115	-7.0	-18.17
OI40/7c3	50	905	428	-7.0	-18.19
OI40/7c4	30	905	208	-12.0	-18.70
OI40/7c5	30	800	1260	-9.7	-19.60
OI7c1	70	900	120	-7.0	-18.02
OI7c2	70	900	120	-7.0	-18.17
OI7c3	70	900	120	-7.0	-18.07
OI7c5	20	700	11580	-12.0	-20.70
OI7c6	30	750	1080	-12.0	-20.05
OI7c8	30	850	1440	-10.0	-19.34
OI7c9	30	950	120	-10.0	-18.34
OI7c10	30	1000	126	-10.0	-17.74

The RBS spectra were simulated with the software RBX (Version 5.18, Kotai 1994). The spectra were fitted with this program by an iterative procedure. Once a best fit is found to calculate the appropriate stopping power a true concentration-depth profile for Fe is extracted, which is then modeled to extract diffusion coefficients. More details of the fitting procedure and the sensitivity of our setup are given in Dohmen et al. (2002) or Tirone et al. (2005).

Results

Nano-scale texture (geometry) and chemistry of thin films

Detailed observations of the geometry and chemistry of the thin films, before and after pre- as well as diffusion anneals

reveal that depending on temperature, composition and other factors the films may behave differently. It is necessary to identify and distinguish between these scenarios to model diffusion profiles with initial and boundary conditions appropriate for each case. It will become evident through the following discussion that using the same diffusion model for all samples over the wide range of temperature and composition would invariably lead to artifacts.

The initial thin film compositions as measured with RBS are listed in Table 2. It shows that many films have a stoichiometry which deviates significantly from that of an ideal olivine. There is systematically a slight excess of SiO_2 , if the thin films were either deposited using a laser of wavelength 193 nm and/or if the samples were heated moderately (up to 620°C) during deposition. The reasons for the fractionation when using the 193 nm wavelength laser are unclear so far, but using this laser has certain advantages (see Dohmen et al. 2002). Heating of the sample may lead to different sticking coefficients for different ions, which probably explains the fractionation effects observed in hot depositions.

After the pre-anneal of selected samples oriented along [001], we have observed exsolution of SiO_2 on the initially polished surface with RBS. In the reflected light microscope these exsolutions are visible as small dots. The effective thickness of this SiO_2 -layer on the surface varies between 15 and 30 nm as measured with RBS. During the subsequent diffusion anneal, reaction of such a film with SiO_2 was expected to form orthopyroxene and sometimes such orthopyroxene was actually observed. Furthermore, the SiO_2 -layer sometimes completely covered the surface and prevented any Fe–Mg exchange between thin film and substrate, demonstrating that pre-annealing of samples before diffusion experiments may not always be a desirable procedure. Samples oriented along [100] or [010] probably experienced a similar exsolution of SiO_2 during the pre-anneal, but on surfaces that include a component of [001], perpendicular to [100] or [010], because of faster kinetics along that direction. On the polished surface of these samples we have not observed any significant change after the pre-anneal.

The amount of excess SiO_2 in the films (with/without any exsolved SiO_2 from the crystal) is such that in chemical equilibrium the thin film would be a mixture of olivine and orthopyroxene in differing modal abundance. Thus, we conclude that in all these cases, the activity of SiO_2 would be fixed by the coexistence of olivine and orthopyroxene, if the film were to crystallize completely. Therefore we argue that the excess of SiO_2 in the film does not influence our experiment in any uncontrolled way and is in fact beneficial in terms of controlling the thermodynamic environment.

All thin films, whether heated or not during deposition, were amorphous before the diffusion anneal. There were no grains visible in the SEM images of the reference samples and no EBSD pattern could be obtained (see also Dohmen et al. 2002). However, a hot deposition might initiate small nuclei and thereby enhance crystallization rates during the subsequent diffusion experiment. Thin films made from Fo_{80} -targets crystallize rapidly (i.e. on a time-scale that is short compared to the overall duration of the anneal) during the diffusion anneal only if temperatures are significantly higher than 900°C. The initially amorphous thin films become a compact polycrystalline matrix with grain sizes in the range of 50–200 nm (Fig. 1). A special situation arises when the film does not crystallize within diffusion time scales. Here, the chemical potential of Fe_2SiO_4 in the more Fe-rich amorphous film can be equal to or even lower than the corresponding chemical potential in the single crystal, leading to no effective diffusive flux or even a small flux of Fe out of the crystal. These situations were observed for thin films with a Fo_{80} composition at diffusion anneals $\leq 900^\circ\text{C}$, in particular if samples were oriented along the *c*-axis. Therefore in this lower temperature range we have performed experiments with films that are much richer in the fayalite component (Fo_{30} or pure fayalite), to ensure a strong chemical gradient between film and substrate even when the film is still amorphous. However, the film crystallizes more rapidly when it is fayalite-rich, as can be seen in Fig. 1d, e. Therefore, we go from a situation with flux of Fe out of the olivine to an amorphous Fo_{80} film to one with flux into olivine from a crystalline Fo_{30} film under a strong gradient. There is a further complication that arises with Fe-rich films. In the case of the Fe-rich Fo_{30} or fayalite films, we had to use films of only about 30–50 nm thickness (Table 2) because the crystallized film of these Fe-rich compositions de-wets areas (Fig. 1e), which has to be considered for the interpretation of the RBS spectrum. Spectra from de-wetted areas with thicker films (>100 nm) become impossible to interpret.

Even when the grain sizes in the crystallized film are in the 100 nm range the surface topography is much smaller as long as the film completely covers the surface (i.e. no de-wetting). Quantitative analysis with the IFM shows that the maximum height variation is ± 10 nm and that the average roughness of the thin films is less than 3 nm (Fig. 2), which is well below the depth resolution of RBS (5 nm). That means the geometry of the thin film diffusion couple is well defined for getting a reliable depth profile measurement using RBS. Any pronounced topography of the thin film would lead to convolution effects in the RBS analysis and artificial diffusion profiles could be the result. Data from samples that for any reason have developed a roughness on the order of the diffusion profile length have not been considered.

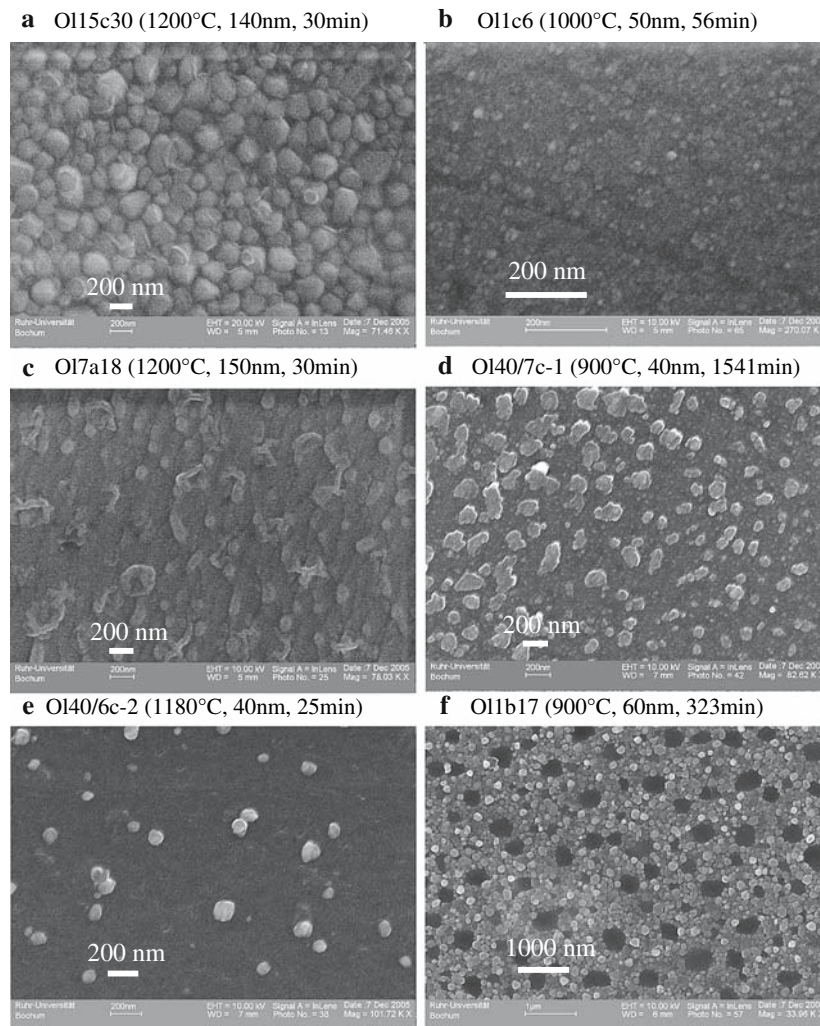


Fig. 1 Highly resolved SEM images of re-crystallized thin films (top view) of six different samples. Note that depending on the initial stoichiometry (see Table 1) and thickness, differing textures can be observed. For instance in the case of OI15c30 (140 nm thick layer) **a** uniform compact polycrystalline matrix with olivine grains between 50 and 200 nm in size has formed in less than 30 min at 1200°C; **b** had only a 50 nm thick layer with olivine stoichiometry and the grain size varies correspondingly between only 10 and 60 nm, which formed at 1000°C in less than 50 min. A completely different texture can be found for samples that have an excess of either (Fe + Mg)/Si-

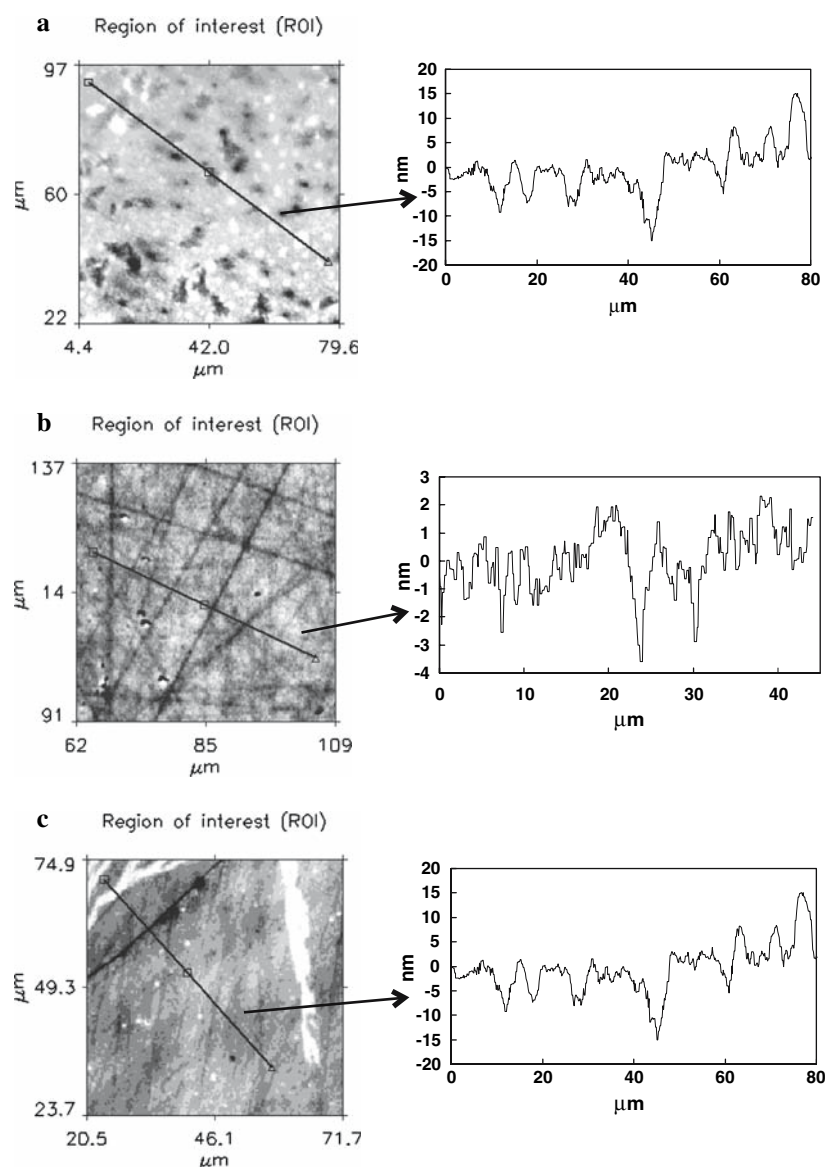
ratio **c** or Si/(Fe + Mg)-ratio **d**, **e**—crystals of differing morphology can be observed and some objects might be brighter or darker not just because of the topographical contrast, but because of a different chemistry (heavier elements, e.g. more Fe or more Si than olivine). The IFM images (Fig. 2) confirm this interpretation, because they show that the surface topography of these samples is extremely smooth, with an average roughness of less than 3 nm. Another phenomenon can be observed in the case of the pure and thin fayalite films (samples OI1b17–20) where due to crystallization the film dewets the surface and forms open areas (**f**)

Although the surface topography is relatively flat, some thin films show a chemical heterogeneity after the diffusion anneal, which is inferred from the SEM images (Fig. 1), because the lighter regions are believed to be caused by a chemical and not a topographical contrast. This is expected for samples where the film did not have a pure olivine stoichiometry. The different objects/crystals identified in the SEM image are too small to be analyzed using EDX in the SEM.

The RBS spectra from different kinds of samples are shown in Fig. 3. We refer the interested reader unfamiliar

with RBS to figures in Dohmen et al. (2002) as well, where the variation in RBS spectra of olivine due to variations in different parameters (thickness, stoichiometry etc.) has been illustrated. RBS analysis of thin films with a chemical heterogeneity reveal of course only an average chemical composition of the film, because of the low lateral resolution of 0.5 mm. Nevertheless a depth distribution of the chemical composition in the film is observed, which cannot be explained just by zoning of Fe–Mg (e.g. Fig. 3b) in all cases. For example, regions in the film which were clearly enriched in SiO₂ or (Mg, Fe)O compared to an olivine

Fig. 2 Surface topography measured with the interference microscope (IFM) for three different samples and the corresponding topographic profiles along one chosen line (black line in image). For the comparison with the SEM images of the same samples one has to consider that the lateral resolution of interference microscopy is much less than that of SEM, a maximum of about 200 nm. The average surface roughness of the samples calculated by the software ATOS Mark II V3.7.15 are as follows: **a** 2.4 nm (O115c30), **b** 0.7 nm (O11c6), and **c** 0.6 nm (O17a18). The most apparent difference compared to the SEM image is that scratches on the substrate due to the polishing are still visible for sample O11c6 with a film of a thickness less than 100 nm. Moreover these scratches still dominate the surface topography. From this, we can make two major conclusions—first, the thin film follows the surface topography of the substrate and re-crystallization of the film does not change the surface topography significantly and second, the sensitivity or resolution of the SEM image at this height scale is much lower than that of the interference microscope (about 1 nm) and the contrast observed in the SEM images is mainly due to chemical effects



stoichiometry were identified. In some cases the chemical composition of the thin film can be separated into two sub-layers, e.g. one with a composition closer to olivine and one closer to orthopyroxene. Nevertheless, because the geometry of the film is well defined, contributions from the film and the substrate single crystal olivine to the RBS spectrum can be clearly differentiated. Most notably, actual analysis of the chemical zoning (as opposed to boundary conditions for diffusion, see below) in the single crystal should not be affected by any chemical heterogeneity in the film. Therefore, as long as the suitable initial and boundary conditions are used in each case, the retrieved diffusion coefficients would be reliable.

In summary, we conclude that the analysis of the diffusion profile in the olivine single crystal as well as the diffusion process itself is not influenced in any

uncontrolled manner through the irregularities (crystallinity, composition and phase assemblage) in the thin film. The fact that the irregularities can be detected and quantified means that suitable boundary and initial conditions can be used for modeling the diffusion profiles in each case. The point defect chemistry of the olivine single crystal is influenced when the activity of SiO_2 is defined by the composition (excess silica) of the film.

Fitting of diffusion profiles and compositional dependence

The Fe concentration depth profiles extracted from the RBS spectrum were fitted using either analytical or numerical solutions to the diffusion equation with the appropriate boundary conditions. The diffusion couple

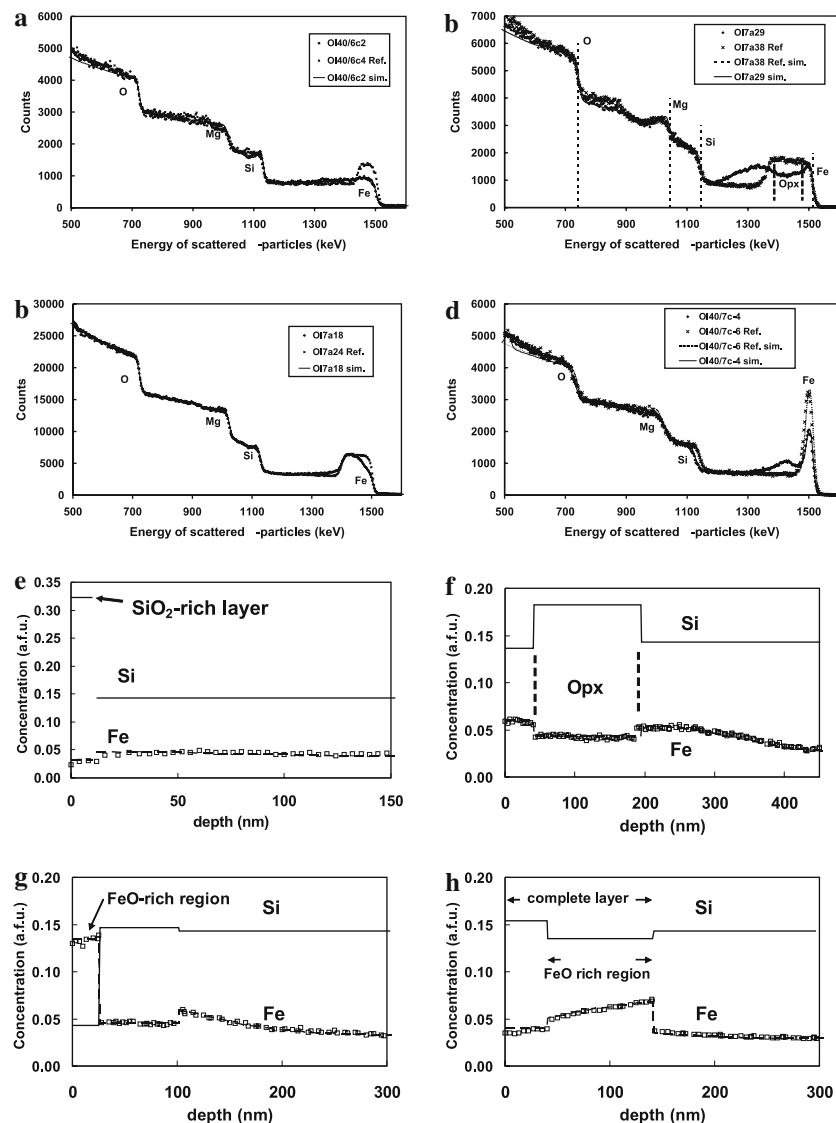


Fig. 3 a–d RBS spectra (symbols showing counts of α -particles as a function of their energy) of four samples along with those from each of the corresponding reference (i.e. unannealed) samples. Simulations of the spectra are also shown as lines. The vertical dashed lines with element symbols in **b** indicate the characteristic energy of alpha-particles of the element when it is scattered back from the surface atomic layer of the sample, these are intended to provide a frame of reference. e–h Concentration depth distributions of Fe (dashed line) and Si (solid line) used as input to obtain the simulations for the spectra of annealed samples shown in a–d. Symbols in e–h show the extracted Fe concentration profile from the spectra using the software RBX (see text), which matches in general the input data for Fe very well. The concentration unit a.f.u. stands for number of atoms per formula unit of the olivine substrate M_2SiO_4 . Within the layer the stoichiometry can deviate significantly from that of olivine, but the unit is always equivalent to atom%/100. The four different samples shown here represent the four different kinds of situations identified

using SEM and RBS: **a** and **e**. An almost ideal situation (sample OI40/6c-2)—a smooth but very flat profile and pure olivine stoichiometry in the film, but with a top SiO_2 -rich layer; **b** and **f** sample OI7a29, excess of Si to Fe + Mg leads to formation of Opx in the layer. In the RBS spectrum the Fe signal in the film is lower in the Opx region (highlighted in the figure), because in Opx, Fe in a.f.u. units is smaller than that in olivine for the same X_{Fe} . **c** and **g** samples OI7a18 and reference sample OI7a24, excess of Fe + Mg to Si leads to formation of magnesioferrite and reduces the Fe content in the olivine of the film. The result is a relatively flat profile in the substrate and an apparent compositional jump between substrate and film; **d** sample OI40/7c-4 and reference sample OI40/7c-6, absolute Fe-rich layer with SiO_2 excess leads to formation of an opx and ol mixture after crystallization. Here, the film has not yet completely crystallized after the short anneal (116 min) at $900^\circ C$, which leads to a partitioning of Fe and Mg between ol, opx and the amorphous phase (Fe-rich layer at the surface)

(thin film + substrate) can be treated as a linear composite semi-infinite medium. The analytical solution for a one-dimensional system with a layer of finite thickness

(constant diffusion coefficient, D_{film}) with zero flux at the surface on a semi-infinite substrate (constant diffusion coefficient, D_{sub}) is given by Lovering (1936): The

analytical solution for a one-dimensional system with a layer of finite thickness (constant diffusion coefficient, D_{film}) with zero flux at the surface on a semi-infinite substrate (constant diffusion coefficient, D_{sub}) is given by Lovering (1936):

$$\frac{C_{\text{film}}(x, t) - C_{\text{sub}}^{\circ}}{C_{\text{film}}^{\circ} - C_{\text{sub}}^{\circ}} = -\frac{1+p}{2} \cdot \operatorname{erf}\left(\frac{x}{2 \cdot \sqrt{D_{\text{film}} \cdot t}}\right) + \frac{1+p}{2} \cdot \sum_{n=1}^{\infty} (-p)^{n-1} \cdot \left[\operatorname{erf}\left(\frac{d \cdot n + x}{2 \cdot \sqrt{D_{\text{film}} \cdot t}}\right) - p \cdot \operatorname{erf}\left(\frac{d \cdot n - x}{2 \cdot \sqrt{D_{\text{film}} \cdot t}}\right) \right]$$

$$\frac{C_{\text{sub}}(x, t) - C_{\text{sub}}^{\circ}}{C_{\text{film}}^{\circ} - C_{\text{sub}}^{\circ}} = -\frac{1-p}{2} \cdot \operatorname{erf}\left(\frac{x}{2 \cdot \sqrt{D_{\text{sub}} \cdot t}}\right) + \frac{(1-p^2)}{2} \cdot \sum_{n=1}^{\infty} (-p)^{n-1} \cdot \operatorname{erf}\left(\frac{d \cdot \sqrt{D_{\text{sub}}/D_{\text{film}}} \cdot n + x}{2 \cdot \sqrt{D_{\text{sub}} \cdot t}}\right)$$

$$p := \frac{\sqrt{D_{\text{film}}} \cdot D_{\text{sub}} - \sqrt{D_{\text{sub}}} \cdot D_{\text{film}}}{\sqrt{D_{\text{film}}} \cdot D_{\text{sub}} + \sqrt{D_{\text{sub}}} \cdot D_{\text{film}}}$$

where h = film thickness and $d = 2 \cdot h$, and represent the initial concentration at $t = 0$ in the thin film and the substrate, respectively. The variable x is the distance from the film/substrate interface with $x > 0$ for the substrate.

A fit of an Fe concentration depth profile after a diffusion anneal with a diffusion couple consisting of a Fo_{80} thin film on a Fo_{95} substrate (O11c) using the above analytical solution is shown in Fig. 4a. For the film a separate faster diffusion coefficient is chosen, because in the polycrystalline film with nano-scale grains there is a significant contribution from grain boundary diffusion. As a consequence the concentration within the film is homogeneous (Fig. 4), which requires a diffusion coefficient, D_{film} , which is about one to two orders of magnitude faster than D_{sub} . This defines only a lower limit for D_{film} , the profiles in the substrate could be simulated with very similar (see below) values of D_{sub} for any other larger value of D_{film} . Consequently, from the profiles effective diffusion coefficients for the polycrystalline films could not be extracted. For those samples that show a chemical heterogeneity in the film it was not possible to observe a perfect fit of the composition in the film, because the zoning is also due to an averaging of compositions of olivine and excess SiO_2 or orthopyroxene. In this case a bulk average of the film composition was calculated and the zoning in the substrate was fitted. The bulk average concentration was always used as a constraint for mass balance—Fe lost from the film (as the initial composition is well known) has to end up in the single crystal substrate. Herein lies a major strength of this approach with films whose initial and final states are well characterized—if any process other than diffusion occurs

during the experiments, it would manifest itself through a violation of mass balance based on the diffusion equation. In any case, the films always worked as a finite diffusion source, where diffusive transport through the film was faster than within the substrate and a set of fitting parameters where D_{sub} is defined within ± 0.1 to 0.2 log units and $D_{\text{film}} \gg D_{\text{sub}}$ can be used to obtain reasonable visual fits.

Since Fe–Mg diffusion depends strongly on composition (approximately an increase of three orders of magnitude from pure forsterite to pure fayalite, Chakraborty 1997) the above analytical solution is not appropriate if the initial chemical gradient exceeds much more than 10 mol% forsterite content. In these cases with relatively Fe-rich thin films we have chosen a finite difference scheme to solve the diffusion problem numerically (see e.g. Crank 1975). Examples of such fits are shown in Figs. 4b and 5.

For a thin film diffusion couple, the effect of the compositional dependence of diffusion coefficient is different from that seen in a couple using two effectively infinite single crystals (see for example Chakraborty 1997). The composition of the thin film changes during the diffusion anneal—the fayalite content and therefore the chemical gradient and the compositional range spanned by the couple becomes smaller with time. Therefore, we have chosen to carry out a time series of experiments at 900°C at constant $f\text{O}_2$, and fitted all profiles with the same compositional dependence, to get self-consistent data for each of the three main crystallographic axes (Experiments O140/7c1–3, O17a24–25, O17b24–26). To describe the dependence of diffusion rates on the fayalite content, based on observations of Chakraborty (1997), we have chosen an exponential form:

$$D(X_{\text{Fe}}) = D(X_{\text{Fe}} = 0) \cdot 10^{n \cdot X_{\text{Fe}}}, \quad (1)$$

where the exponent n is a measure of the compositional dependence. Best fits to a profile for various exponents are shown in Fig. 5. The fits illustrate that the estimation of the exponent from fitting profiles is not very sensitive—only slight changes in the slope of the profile are the result of the compositional dependence of the diffusion coefficient. However, it is this slope at a given position that enters into the calculation of compositional dependence of diffusion coefficients in a Boltzmann–Mantano analysis. Therefore the result of such an analysis is strongly dependent on the accuracy of the profile measurement and especially for strong compositional dependencies, long profiles (i.e. a high density of data points within the diffusion zone) are needed to extract reliable diffusion coefficients. Since this requirement is not always fulfilled in the case of concentration profiles measured using RBS in our study, we have chosen a forward modeling approach to determine the compositional dependence of the diffusion coefficient.

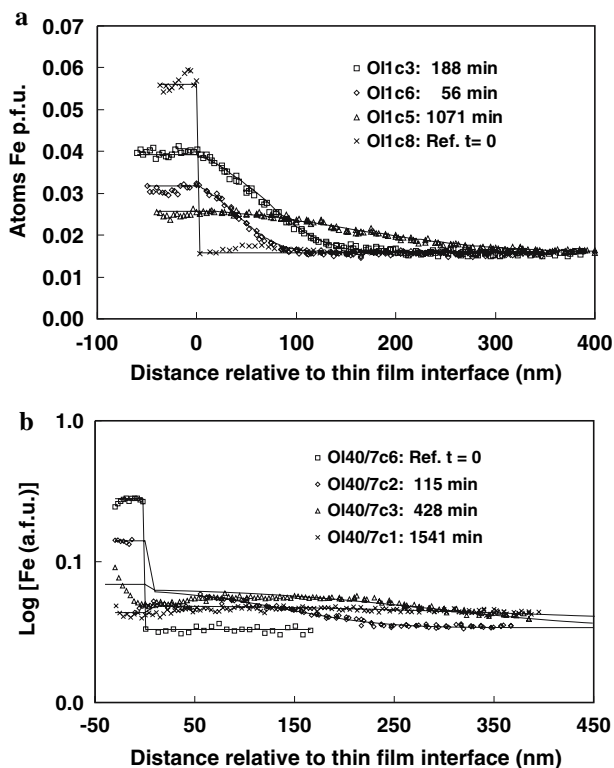


Fig. 4 Illustration of concentration profiles from two sets of time series experiments. Fe concentration depth profiles extracted from RBS spectra for four samples at each condition, and their best fits using the analytical model (a) or numerical modeling (b) considering a concentration dependent diffusion coefficient for the finite difference scheme. **a** The samples (OI1c3, 5, 6) were annealed at 1005°C at an oxygen fugacity of 10^{-10} Pa, but for different durations (see legend in the figure). Note that sample OI1c3 was not deposited together with OI1c5, 6, and 8 and has a thicker film (Table 1), which is reflected in the larger concentration in the film after the diffusion anneal compared to OI1c5 or 6 because of the larger reservoir. **b** The samples OI40/7c1, OI40/7c2 and OI40/7c3 were annealed at 900°C at an f_{O_2} of 10^{-7} Pa for different durations as indicated in the legend. From the depth profiles it is apparent that the thin film does not act either as an infinite source (constant surface composition) or as an instantaneous finite source (like in a), but its behavior as a diffusion source changes systematically during the experiments. Further complications for the interpretation of the depth profiles arise from the fact that RBS yields only a mixed analysis of an amorphous phase, orthopyroxene and olivine in the film. This might influence the depth profile to depths deeper than the initial film thickness depending on the geometry/texture of the thin film, which could be controlled by the grain size of the opx crystals (compare with Fig. 1d). Nevertheless from numerical fitting of the profiles considering the appropriate boundary conditions consistent diffusion coefficients ($-18.27 < \log(D_{FeMg}) < -18.17$) for the substrate composition, Fo₈₈) for the three experiments has been obtained. For more details see text, Tables 1 and 2

However, relatively independent of the exponent used for the fitting one obtains almost the same diffusion coefficients for the substrate composition (Fig. 5). This is because diffusion within the flat part of the profile, where diffusion is slowest, is the rate-determining step for the

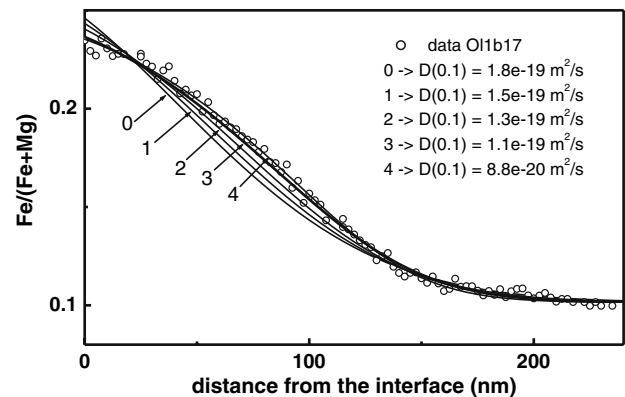


Fig. 5 Illustration of the effect of the chosen compositional dependence (exponent n) on the quality of fit and the extracted diffusion coefficient for the substrate composition. Shown are various fittings for sample OI1b17 that had a pure fayalite thin film before the start of the diffusion anneal. The numbers in the legend from 0 to 4 are the exponents, m , used for the fitting. Also shown within the figure are the diffusion coefficients obtained from any given fit for the given substrate composition. The best fit gives an exponent m between 3 and 4 and a $D(X_{Fo} = 0.9)$ of about 9.0×10^{-20} m²/s

diffusive penetration of Fe into the crystal. Therefore in spite of the large error in the determination of the compositional dependence, the diffusion coefficients determined for the substrate composition (about Fo₉₀) are well constrained. In general, the error for the determination of the diffusion coefficients estimated from various visual-fittings are of the order of ± 0.2 log units, in some cases of very flat or short profiles the error can be up to ± 0.3 log units. We would also like to draw the attention of the reader to this relative insensitivity of profile slopes to compositional dependence for later discussion of diffusion data in the literature (e.g. that of Buening and Buseck 1973).

Satisfactory fits to all profiles are observed with an exponent $n = 3$, which is similar to that observed at 1,000°C ($n = 2.8$) and 1,100°C ($n = 2.6$) by Chakraborty (1997) in his setup using two single crystals in the diffusion couple. Thus, for fitting concentration profiles from the Fa–Fo₉₀ and Fo₃₀–Fo₉₀ diffusion couples we have consistently used a compositional dependence exponent of 3. Table 3 reports diffusion coefficient for Fo₈₆ obtained using this compositional dependence.

Anisotropy and activation energy

Figure 6a–c shows Arrhenius plots of diffusion coefficients measured along [001], [100] and [010], respectively, at an f_{O_2} of 10^{-7} , 10^{-10} and 10^{-12} Pa (only [001]). Note that the stability of olivine aside, at temperatures below 900°C it is impossible to control an f_{O_2} of 10^{-7} Pa using a CO–CO₂ gas mixture because the CO content of such a mix has to be less than 1%. To measure the activation energy at lower

temperatures a set of experiments between 800 and 1,050°C at an fO_2 of 10^{-10} Pa and between 700 and 900°C at an fO_2 of 10^{-12} Pa have been performed. The diffusion coefficients along [001], [100] and [010] are shown in different plots for clarity, in particular because data for [100] and [010] are effectively the same and would plot on top of each other in one plot. Independent of temperature (between 800 and 1,200°C), in all experiments where crystals with surfaces polished perpendicular to [100], [010] and [001] were annealed simultaneously the retrieved diffusion coefficients along [100] and [010] were identical within error (0.2 log units) and diffusion along [001] was a factor of 4–8 times faster.

The data along [001] for 10^{-7} Pa coincide with the data of Chakraborty (1997) and Petry et al. (2004), who also measured diffusion coefficients at an fO_2 of 10^{-7} Pa (Fig. 6a), but with a different setup—two single crystals as diffusion couple and profile analysis with an electron microprobe. Chakraborty (1997) measured diffusion coefficients down to 980°C and mainly at a single fO_2 of 10^{-7} Pa. A bulk fit of all data shown in Fig. 6a, which were measured with San Carlos olivine between 900 and 1,250°C at an fO_2 of 10^{-7} Pa gives an activation energy of 201 ± 8 kJ/mol, slightly lower than 226 ± 18 kJ/mol obtained by fitting the data of Chakraborty (1997) alone. Within the statistical error of the different fits, the activation energies observed from data along [010] and [100] at an fO_2 of 10^{-7} and 10^{-10} Pa are approximately the same. This is represented by the almost parallel lines in Fig. 6, which confirms that the anisotropy is essentially independent of temperature within the temperature regime 800–1,200°C. However, fitting the data measured along [001] at 10^{-10} and 10^{-12} Pa together with the activation energy is about 20 kJ/mol larger (220 ± 9 kJ/mol), which may be an important indicator for the temperature dependence of the point defect chemistry in olivine as will be seen in Part II.

In Fig. 6a–c it is also indicated which kind of crystal was used for each experiment. Basically it was differentiated between O11 (Nanga Parbat) and San Carlos olivine, and it can be seen that the data points for different crystals all fit into the overall picture independent of the nature of the crystal. The only exception is data from olivine O11c. The olivine O11c differs significantly in its composition compared to the other olivine crystals used (Table 1) in that it has higher forsterite content (95 mol%), and the concentrations of Al_2O_3 and Cr_2O_3 are much smaller. The Fe–Mg diffusion coefficients in these samples are slightly (about 0.5 log units) but significantly smaller than data from, for example, O140c or O17c at the same conditions. This difference cannot be attributed to the dependence of diffusion rates on the fayalite content alone, the “impurities” (Al and Cr) may be the reason behind this discrepancy. In Part II we will provide a quantitative explanation

for this behavior. For the derivation of activation energies and fO_2 dependence the data of O11c have not been considered to obtain a self-consistent data set for an olivine with a more or less typical composition (compare with Table 1).

Dependence on fO_2

All experimental studies on Fe–Mg diffusion in olivine so far have found a positive dependence of diffusion rates on oxygen fugacity. This is expected according to the point defect model of Nakamura and Schmalzried (1983) for the case of a vacancy diffusion mechanism. The concentration of octahedral vacancies increases with increasing fO_2 because the partial oxidation of Fe^{2+} to Fe^{3+} is charge balanced by the formation of these vacancies. But the exact dependence (expressed by an exponent m : $[V_{Me}] \sim D_{FeMg} \sim (fO_2)^m$, all other relevant intensive thermodynamic variables remaining constant) depends on the majority defects and whether the activity of SiO_2 is held constant (Stocker and Smyth 1978; Barkmann and Cemic 1996; Part II). In principle, an accurate determination of the exponent would enable one to distinguish between different point defect models (charge neutrality conditions) for olivine (Schmalzried 1981).

In the last section the effect of fO_2 was shown for three different oxygen fugacities at relatively low temperatures. Here, the observed dependence (exponent $m \sim 1/6$ – $1/8$ between 10^{-7} and 10^{-10} Pa, no effect between 10^{-10} and 10^{-12} Pa) is weaker compared to various other studies (Buening and Buseck 1973; Nakamura and Schmalzried 1984; Petry et al. 2004) and what would be expected from point defect models for pure and synthetic olivine (Nakamura and Schmalzried 1983; Tsai and Dieckmann 2002). To measure the fO_2 -dependence at higher temperatures as well, we have carried out sets of experiments at 1,080°C (along [001]) and 1,050°C (along [100]) and varied the fO_2 between 10^{-5} and 10^{-11} Pa. At around 1,050°C, we observe a mean dependence of $\log(D_{FeMg})$ on $\log(fO_2)$ given by an exponent m between 1/5 and 1/7 (Fig. 7). For comparison we illustrate in Fig. 7, lines for a dependence with an exponent of 1/4 and 1/6. This illustrates that given the scatter of the data, it is impossible to distinguish clearly between an exponent of 1/4 or 1/6. Therefore the observation is consistent with the general range of fO_2 -dependence found in earlier studies (Petry et al. 2004; Nakamura and Schmalzried 1983, Buening and Buseck 1973, Jurewicz and Watson 1988). However, at 900°C at the more reducing conditions (with respect to absolute numbers for the fO_2) the effect of fO_2 is much weaker; the exponent m lies at around 1/10. At 1,050°C as well, the effect seems to flatten out at the more reducing conditions. These observations indicate that at lower temperatures (equivalent to

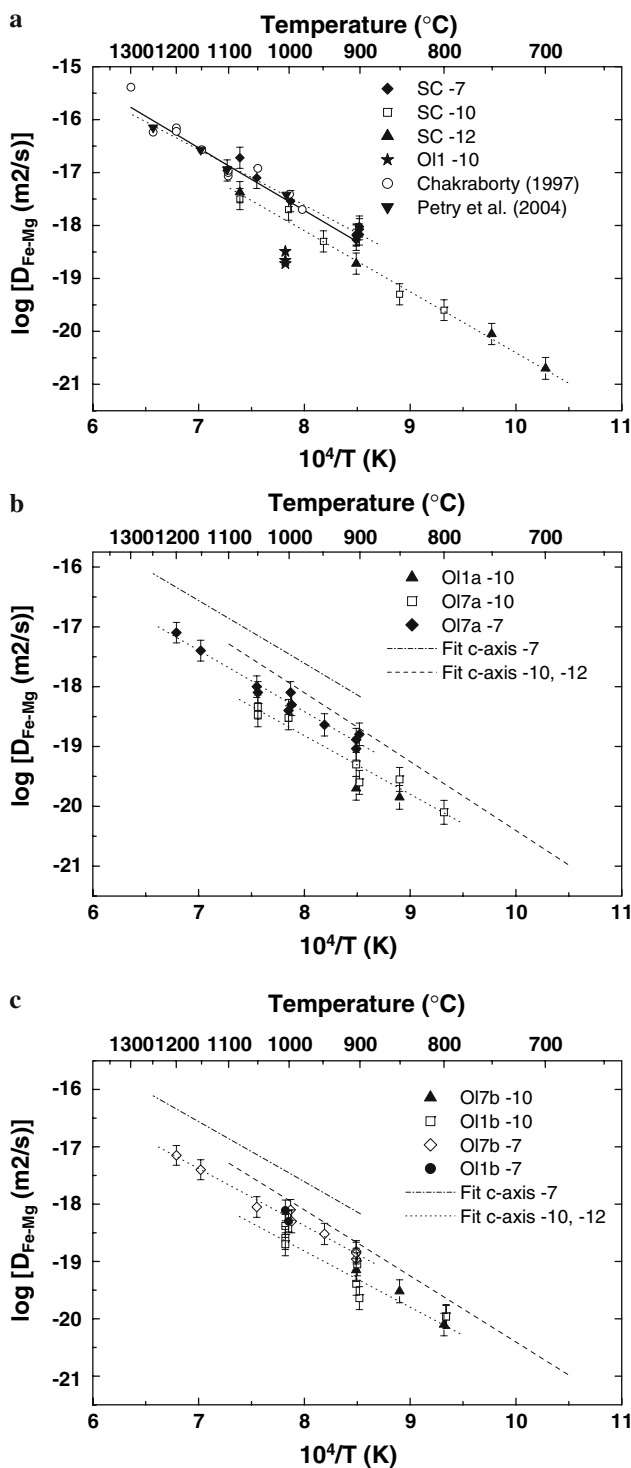


Fig. 6 Anisotropy of Fe–Mg diffusion as a function of temperature. Diffusion coefficients measured for diffusion along **a** the *c*-axis, [001], **b** the *a*-axis, [100], and **c** the *b*-axis, [010], between 900 and 1200°C at $fO_2 = 10^{-7}$ Pa and between 800 and 1050°C at $fO_2 = 10^{-10}$ Pa. Additional data were measured along the *c*-axis for an fO_2 of 10^{-12} Pa between 700 and 900°C. For diffusion along the *c*-axis, the raw data points of Petry et al. (2004) and the Arrhenius fit obtained by Chakraborty (1997) (solid line) are shown in addition in **a**. The dotted line is a fit including the raw data (up to 1250°C) from Chakraborty (1997) and Petry et al. (2004). Data for the *a*- and *b*-axes are shown in separate plots for clarification, because there is no significant difference between diffusion along *a* and *b*. As a reference in these two plots the fits to the data along [001] at fO_2 of 10^{-7} Pa and 10^{-10} – 10^{-12} Pa are included as dashed lines. All data at constant fO_2 and orientation can be fitted by a linear function (dotted lines, least square regression fits) within the whole temperature range. Note that these lines are almost parallel where the slope is equivalent to approximately the same activation energy of about 200 kJ/mol (see text)

Kinetics of point defect equilibrium

An alternative explanation for the absence of any fO_2 dependence could be that the point defect chemistry of olivine is “frozen” at lower temperatures and this possibility needs to be explored before drawing conclusions about changes of diffusion mechanisms. The nature of the diffusion process itself requires that the vacancies always diffuse much faster than the cations and from this point of view the concentration of the vacancies on the M1 or M2 sites should equilibrate quickly compared to Fe–Mg diffusion time scales. However, re-equilibration of vacancies in olivine also requires a net transfer of oxygen, because olivine is a non-stoichiometric phase (see Nakamura and Schmalzried 1983 and part-II for details). This exchange of oxygen with the experimental environment may be kinetically hindered because of the inefficiency of evaporation/condensation processes at low temperatures. If this is the case, then olivines with different histories would yield different diffusivities when annealed at the same lower temperature conditions (e.g. see Bai and Kohlstedt 1993). To test for this possibility, we pre-annealed a set of samples at 1,200°C either at 10^{-7} Pa or at 10^{-2} Pa, deposited them with thin films in the same batch and carried out diffusion anneals at 900°C at $fO_2 = 10^{-7}$ Pa with the samples placed together in the furnace in the same experimental run. The crystals changed their color after the pre-anneal indicating a change in the oxidation state of Fe—those annealed at 10^{-2} Pa became relatively brownish. After the diffusion anneal at 900°C for a relatively short time (2 h) all crystals had the same color and we observed very similar diffusion profiles. The diffusion coefficients obtained from these samples are the same within error (Table 3). Furthermore, we did not observe any difference between data of samples that were pre-annealed or not, all of them fit into the general overall picture of the data, as

lower oxygen fugacities for an fO_2 -buffer) the fO_2 -dependence becomes less important or in fact vanishes. An absence or a weaker dependence of diffusion on fO_2 implies important changes in point defect disorder type and therefore diffusion mechanism in olivine at these lower temperatures, if the defects are in chemical equilibrium with the surrounding.

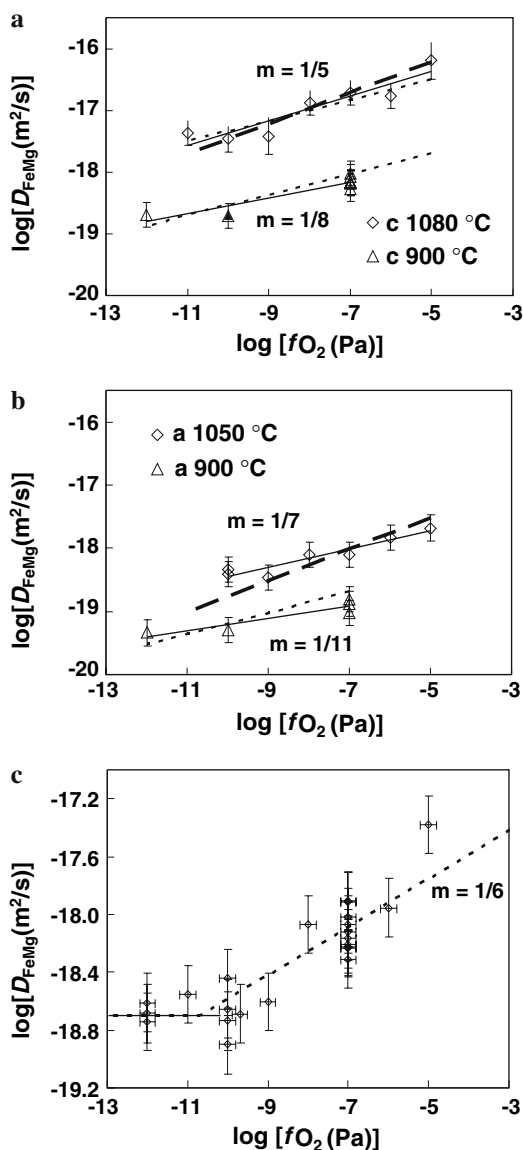


Fig. 7 Effect of $f\text{O}_2$ on diffusion data at two temperatures. **a** Diffusion data at 1080°C and 900°C along [001] at various $f\text{O}_2$. **b** Diffusion data at 1050°C and 900°C along [100] at various $f\text{O}_2$. The straight lines are the least square regression fits of the data at constant temperature and various $\log(f\text{O}_2)$ and the slopes of these fits (m) are given in the figures. The dotted lines show for comparison a $1/6$ dependence on $\log(f\text{O}_2)$, the dashed lines a $1/4$ dependence. These seem to describe the observed data, at least at the higher temperature in each case, rather well. **c** Normalization of all diffusion data measured along [001] to 900°C using an activation energy of 200 kJ/mol for data measured at an $f\text{O}_2 > 10^{-10}$ Pa and 220 kJ/mol for $f\text{O}_2 < 10^{-10}$ Pa. While the normalization concentrates errors from different sources contributing to the scatter, it is seen more clearly here how the dependence of diffusion coefficients on oxygen fugacity decreases at lower oxygen fugacities. The data can be adequately described (based on an analysis of point defect models in Part II) by a region with an $f\text{O}_2$ dependence exponent, m , of $1/6$ and a lower $f\text{O}_2$ region where diffusion is independent of oxygen fugacity. The transition corresponds to a change in diffusion mechanism from TaMED to PED (see text). Note also the smeared nature of the transition

shown before. Thus, we conclude that there was no influence of the individual thermal history of the samples and that point defect equilibrium was attained almost instantaneously during the diffusion anneal. Therefore, the change in $f\text{O}_2$ dependence at more reducing conditions and/or lower temperatures is an equilibrium phenomenon that needs to be discussed in terms of change in the point defect disorder model, we pursue this in Part II.

Discussion and comparison with earlier studies

We commence by summarizing the main findings of this study: the Fe–Mg diffusion coefficient in olivine depends on the composition of the olivine, with a compositional dependence exponent, n , of 3 for olivines of composition $\text{Fo}_{90}\text{–}\text{Fo}_{30}$. The diffusion coefficient in olivine depends on $f\text{O}_2$ above an $f\text{O}_2$ of 10^{-10} Pa and the $f\text{O}_2$ dependence is described by an exponent, m , that lies between $1/4$ and $1/6$ on average between the $f\text{O}_2$ range of 10^{-5} to 10^{-10} Pa. Given the resolution of the data, it is not possible to differentiate between these values of m . All data appear to plot on parallel lines in an Arrhenius plot, where each line stands for a constant $f\text{O}_2$ (see also Petry et al. 2004) and orientation. Considering all data at $f\text{O}_2 = 10^{-7}$ Pa, we obtain almost identical activation energies of 196 ± 12 , 191 ± 9 and 201 ± 8 kJ/mol for diffusion along [100], [010] and [001] in olivine, respectively. These results have the important implication that the anisotropy of diffusion in olivine is temperature independent, at least between 800 and 1,250°C. Moreover, this constant activation energy suggests that a change of diffusion mechanism, e.g. from intrinsic to extrinsic, does not occur in olivine within this temperature range and diffusion coefficients can be reliably extrapolated. Other subtle changes in diffusion mechanism do, however, occur at lower temperatures at reducing conditions, which are probably related to specific impurities and these aspects are discussed in detail in Part II.

In comparing these results with those of earlier studies, we find that the absolute values of diffusivity as well as the preliminary compositional dependence, $f\text{O}_2$ dependence and anisotropy observed by Chakraborty (1997) have been confirmed in this more detailed study covering a much larger range of parameter space. The results of Petry et al. (2004), Meissner et al. (1998) and Dohmen et al. (2003) are all consistent with this study and that of Chakraborty (1997). We note that each of these studies has used a different experimental and/or analytical approach, so that the Fe–Mg diffusion coefficients in olivine have now been measured, and repeatedly reproduced, using a variety of methods. The temperature dependence of anisotropy of diffusion (i.e. different activation energies along different crystallographic directions) found in previous studies

(Buening and Buseck 1973; Misener 1974 and Jurewicz and Watson 1988) has not been confirmed.

For a detailed comparison with other studies, it is necessary to consider the observed dependencies on fO_2 and X_{Fe} . In Fig. 8a, b we have compiled data for diffusion along [001] and [010], respectively. If the data were not reported for an fO_2 of 10^{-7} Pa, we have normalized these data to an fO_2 of 10^{-7} Pa using the dependency obtained in this work. Misener (1974) reports two distinct sets of data (high temperature data measured with a Fe_{90} olivine and MgO diffusion couple, and low temperature data measured with a Fe_{90} -fayalite diffusion couple) and we show both. We want to note here that the author himself restricts the lower temperature data set to olivine compositions with more Fe than in Fe_{80} , and for modeling mantle processes he himself used only the higher temperature data set. Nevertheless, *typical usage of these data in the literature involves extrapolation of his low temperature data in compositional space to Fe_{90} -olivine*. Therefore, we show

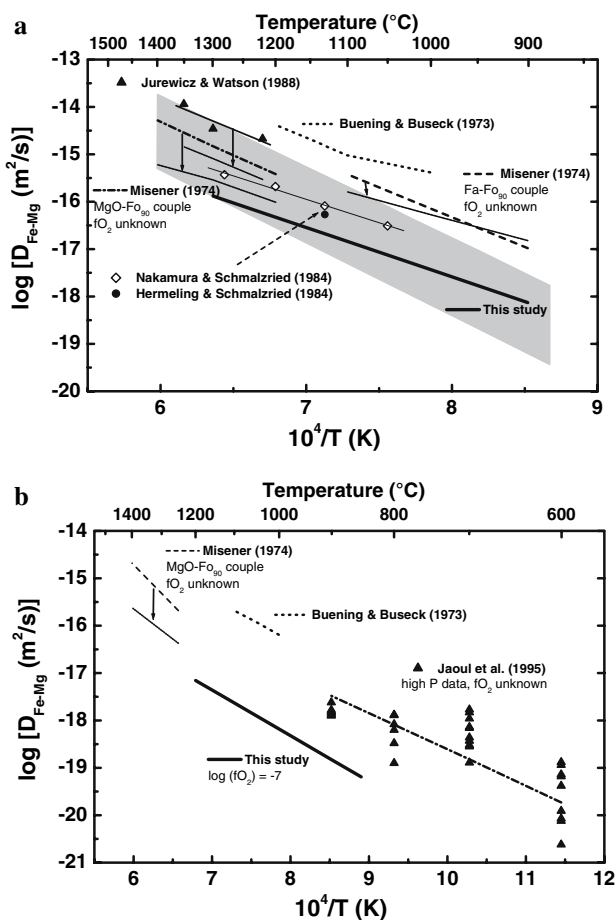


Fig. 8 Comparison of best fit to our data with data for Fe–Mg diffusion along the *c*-axis (**a**) and the *b*-axis (**b**) from the literature. All data were normalized to an fO_2 of 10^{-7} Pa using an exponent of 1/6 and to a forsterite content of 86 mol%. For more details of data reduction see text. The sources of the data are indicated in the figure

both sets of data on one plot. Unfortunately, fO_2 was not explicitly controlled in his study, so we have estimated it based on his experimental setup. In the fayalite-rich setup quartz tubes were filled with the diffusion couples and these experiments might have been close to the FMQ buffer. In Fig. 8 we have plotted the raw data as well as the “ fO_2 -corrected” data assuming that the fO_2 was at the FMQ buffer. The high temperature data, valid for Fe_{90} , were produced in a different setup using MgO or forsterite as exchange partner for an Fe_{90} olivine and an fO_2 cannot be easily estimated. As it stands, the data are about an order of magnitude faster than those found in this study; if it is assumed that the FMQ buffer applies for the fO_2 correction, the data show a perfect agreement with that of Chakraborty (1997) and this study. The data of Nakamura and Schmalzried (1984) were measured using synthesized polycrystalline pellets as diffusion couples and therefore measured concentration profiles should have a contribution from grain boundary diffusion of Fe and Mg. In the case of olivine, grain boundary diffusion is about a factor of 1,000 faster than volume diffusion (Farver et al. 1994). For the given grain size between 30 and 50 μm the system would show a Type-B behavior according to the classification of Harrison (1961) and therefore grain boundary diffusion would have had a significant influence on the compositional profile. The main result would be an enhancement of the diffusive transport through the pellet and retrieved diffusion coefficients would be higher than volume diffusion coefficients by up to a factor of 10. A further source of error, that works in the opposite direction, is that the grains in such a polycrystalline mix are not oriented so that the average diffusion rate would be one between the rates along the faster [001] and the other slower directions. Considering these effects, the factor of 5 faster diffusion observed by them, compared to data from this study and those of Chakraborty (1997) is reasonable. In addition we have shown one data point for tracer diffusion of Fe, D_{Fe}^* , determined by Hermeling and Schmalzried (1984). For Fe -rich olivine the tracer diffusion coefficient of Fe should be close to the interdiffusion coefficient, if one considers the Mg tracer diffusion data of Chakraborty et al. (1994). Indeed, the Fe tracer diffusion coefficient, measured in a similar polycrystalline matrix, is very similar.

In the work of Jurewicz and Watson (1988) data were collected at an fO_2 of 10^{-3} Pa and again we have shown in Fig. 8 the original fit of the data for Fe at 10^{-3} Pa as well as the normalized fit for 10^{-7} Pa. Here, we observe a similar difference as for Nakamura and Schmalzried (1984) of about a factor of 5. Jurewicz and Watson (1988) investigated diffusion in olivine using surrounding melts as the exchange partner. Among other features, self-buffering reactions in the melt may have controlled the oxygen fugacity of these experiments, rather than the imposed gas

mixtures. Further, dissolution and precipitation processes might have played an important role in creating dislocations and these could have enhanced diffusion by mobilization. We have been able to reproduce their data in a similar setup for diffusion (Düffels et al. 2004) and explanation of these results will be presented in detail elsewhere. Taking data from this study as a point of departure, in Fig. 8a we also show the range over which diffusion coefficients could lie for variations in oxygen fugacity across the entire stability field of olivine (see Part II) at each temperature. It is seen that all of the above data sets could be obtained through a combination of variation of oxygen fugacity and other experimental factors outlined above. The only exception is the detailed study of Buening and Buseck (1973), with which we concern ourselves in the next section.

Effect of the lateral resolution of the microprobe analysis on the data reduction of Buening and Buseck (1973)

The only results from high temperatures that differ strongly from this study and Chakraborty (1997) are those of Buening and Buseck (1973). They used fayalite powder as the source material for diffusion into San Carlos olivine and assumed this to be an infinite reservoir. Compositional profiles were measured with an electron microprobe in 2 micron steps just in the single crystal part of the samples. In Fig. 1 of Buening and Buseck a compositional profile for a sample annealed at 1,100°C for 242 h is presented. When compared to the shape of the profile measured by Chakraborty (1997) on a sample annealed at 1,000°C for 208 h (Fig. 2a) for a similar diffusion couple, it is evident that the latter is much more asymmetric. The strong asymmetry follows from the strong compositional dependence of Fe–Mg diffusion in olivine found in many studies (e.g. Nakamura and Schmalzried 1984; Hermeling and Schmalzried 1984; Misener 1974; Dohmen et al. 2003; Chakraborty 1997 and this work). All the cited references found an exponent n between 2 and 3 (Eq. 1). The implication of this is that in addition to the difference in the absolute values of diffusion coefficients they retrieved, Buening and Buseck (1973) also observed a much weaker compositional dependence (exponent n of only 1.6) than in any of the other studies. This smoothing of compositional gradients as well as the shape of their profile points strongly to a convolution effect in their microprobe analysis, a possibility already discussed in Chakraborty (1997). Here, we have carried out a more detailed analysis of the profile shape they obtained.

We have reproduced a scanned version of a compositional profile from Buening and Buseck (1973), their Fig. 1, in Fig. 9. We have superposed on this calculated

profile shapes using various approaches. All profiles were calculated using a finite difference numerical scheme in the forward modeling approach where compositionally dependent diffusion coefficients were used. As boundary condition the concentration at the surface of the crystal was held fixed at the observed value, consistent with the model of an infinite reservoir assumed by Buening and Buseck (1973). We note here in passing that even this assumption has been found to be not valid in experiments in our laboratory carried out to reproduce these data; however, even if the powder material does not act as an infinite reservoir, the composition at the surface of the crystal may remain fixed so that this is not a major shortcoming. Our first calculation (Line #1, Fig. 9) was to use the compositional dependence and diffusion coefficients obtained by Buening and Buseck (1973) from their Boltzmann–Matano analysis (an exponent of 1.6). As is clear from Fig. 9, the match is not very good, highlighting the problems of Boltzmann–Matano analysis and some of the issues of insensitivity of profile slopes to compositional dependence that we have discussed earlier in [Fitting of diffusion profiles and compositional dependence](#). Irrespective of further developments, one aspect may be noted here immediately—underestimating the compositional dependence by one order of magnitude would clearly overestimate the diffusion coefficients for forsterite-rich compositions by one order of magnitude and could explain to some extent the discrepancy of the data of Buening and Buseck from all others.

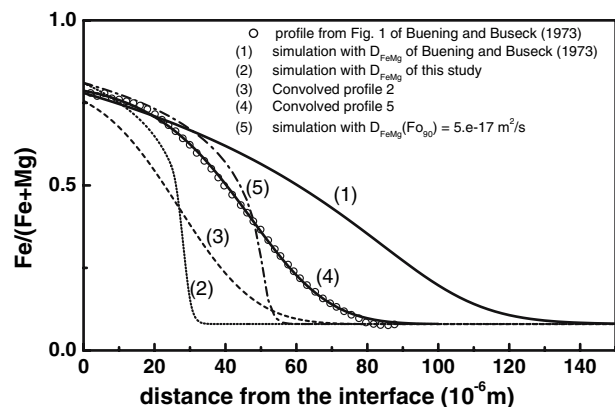


Fig. 9 Reproduction of the concentration profile of Buening and Buseck (1973) from their Fig. 1 (1100°C, 242 h, circular symbols) and our numerical simulations. (1) Profile calculated using the data that Buening and Buseck (1973) have retrieved from this profile using Boltzmann–Matano analysis. (2) Profile calculated using diffusion coefficients retrieved for the same conditions in this study. (3) The result of convolving profile (2) with a convolution factor σ , of 15 μm . (4) Simulation to obtain best fit to measured profile with a convolution factor σ , of 15 μm . This yields a diffusion coefficient of $5 \times 10^{-17} \text{ m}^2/\text{s}$. (5) Unconvolved profile (4), as it would be measured today with a modern electron microprobe

Next (Line 2, Fig. 9), we have calculated a profile for the experimental run conditions of Buening and Buseck (1973) using diffusion data from this study. As expected, the profile is much more strongly asymmetric (compositional exponent of 3) and shorter in length (slower diffusivity). Then (Line 3, Fig. 9), we have tried to convolve this profile, using procedures outlined in Ganguly et al. (1988), to see whether we can match the observed data of Buening and Buseck (1973). For this exercise, we have left the convolution function σ —a measure of beam spreading in the electron microprobe—as a free fitting function. It is found that with a σ of 10–15 μm , we can obtain a fairly good simulation of their profile shape, although the match remains poor. Compared to values of $\sigma = 0.5\text{--}0.6 \mu\text{m}$ determined on modern microprobes, this is a large number (see for example Chakraborty and Ganguly 1992; Ganguly et al. 1996). However, as already discussed by Chakraborty (1997), such large convolution effects are not unrealistic when the low take-off angles of X-rays in older microprobes are considered. For example, re-measurement of profiles from some garnets studied by Rumble and Finnerty (1974) in the 1990s by Ganguly et al. (1996) revealed a convolution effect of exactly this order—a σ value of $\sim 10 \mu\text{m}$. Having established that a simple compositional dependence would never produce the shape of profiles observed by Buening and Buseck (1973) and that convolution of microprobe analysis does produce exactly this shape, we have carried out a final exercise where we have tried to obtain a “best fit” to the observed profile of Buening and Buseck (1973) by simultaneously varying diffusivity as well as the convolution effect. As seen in Fig. 9 (Line 4, which yields Line 5 when stripped of the convolution effect), we succeed in reproducing exactly the shape of profile observed by Buening and Buseck (1973) with a diffusion coefficient (for an olivine composition of Fo_{90}) that is less than half an order of magnitude faster than that found in this study ($\log D = -16.3$), with the same compositional dependence found here, and a convolution function, σ , of 15 μm . Thus we conclude that the much larger diffusion coefficients reported by Buening and Buseck (1973) is a consequence of strong convolution effects in older electron microprobes, compounded by uncertainties of Boltzmann–Matano analysis. When corrected for the convolution effects the data are not any more deviant from the current data set than many others in the literature (Fig. 8). As noted above, such variations of a half an order of magnitude or less may be explained by a number of experimental artifacts, including control of oxygen fugacity. Considering the various sources of uncertainty (e.g. use of polycrystalline material as source and assuming it to be an infinite reservoir), the experiments of Buening and Buseck (1973) need not be considered to be in conflict with those from this study and Chakraborty (1997).

Diffusion along [010]

In a second plot (Fig. 8b) we have compiled the data along [010]. The relation of data obtained in this study to results obtained by Misener (1974) and Buening and Buseck (1973) is the same as for the data along [001]. In addition, the data of Jaoul et al. (1995) determined in the temperature range 600–900°C are shown. The most significant difference to the present study is that these experiments were performed at a high pressure in a piston cylinder or in a multi anvil apparatus. The $f\text{O}_2$ was not explicitly controlled but Jaoul et al. (1995) argue that it was close to the IQF-buffer because of the Fe-metal capsules used in their experiments. They have used fayalite thin films deposited by RF-sputtering as the diffusion source and used RBS as in this study to analyze the Fe depth profiles. High-pressure experiments with thin films are a difficult task, because the film has to survive much more extreme chemical and mechanical conditions than in a gas mixing furnace. The setup developed by Jaoul et al. (1995) helped them to extract single crystals with film after the high-pressure anneal; however, they have not carried out any surface characterization with SEM and interference microscopy. This would be important because our experience indicates (e.g. Chakraborty and Costa 2004) that in such high-pressure experiments substantial re-crystallization of the film occurs leading to larger roughness and substantial convolution effects for any depth profiling method such as RBS. This might be one explanation for the enormous scatter of their data (Fig. 8b). Additional scatter might have been caused by the strong compositional dependence of diffusion rates on the fayalite content. Jaoul et al. (1995) state that they considered this dependence (with an exponent 3, Eq. 1) for the simulation of the RBS spectrum with the software RUMP (Doolittle 1986), but their Table 1 shows that only 3 of 32 profiles were simulated considering this dependence. For the rest of the profiles they assigned the obtained diffusion coefficient to an olivine with a forsterite content “arbitrarily taken at mid-height of the profile” (Jaoul et al. 1995), which introduces a systematic error. A third issue with their data comes from the fact that the concentration profiles they obtained were very flat (small change in the concentration of Fe). Since the initial film thickness was part of their fitting a large variety of diffusion coefficients can be obtained in this case by fitting the same RBS spectrum within its statistical error. Fourthly, Jaoul et al. (1995) did not carry out any time series experiments to exclude any artifacts related to their approach; essentially all experiments were performed for the same time—6 h. Gain of Fe from the Fe capsule may have introduced further artifacts. And finally, such high-pressure experiments may be affected by the influence of water picked up from the cell material, as we have found in our

own studies on Si and O diffusion in olivine. To summarize, there are a number of reasons that may explain the large scatter of their data as well as the larger diffusion coefficients obtained in their study.

Conclusions

We have carried out a set of diffusion experiments with detailed sample characterization to exclude experimental artifacts and obtained Fe–Mg diffusion coefficients in olivines as a function of composition, oxygen fugacity and crystallographic orientation between 700 and 1,250°C. The main findings of this study are:

1. Between oxygen fugacities of 10^{-7} and 10^{-10} Pa, diffusion in olivine may be described by a single activation energy along all crystallographic directions, precluding any change of diffusion mechanism in this range.
2. Activation energies of 196 ± 12 , 191 ± 9 and 201 ± 8 kJ/mol for diffusion along [100], [010] and [001], respectively, in olivine indicate similar temperature dependencies of diffusion along different crystallographic directions and no temperature dependence of diffusion anisotropy. The nature of anisotropy found here has been verified through modeling of natural samples by Costa and Chakraborty (2004) and Costa and Dungan (2005).
3. Diffusion coefficients increase with oxygen fugacity between oxygen fugacities of 10^{-5} and 10^{-10} Pa. The results are consistent with an fO_2 exponent, m , of $1/4$ – $1/6$. Within the uncertainty of measurement, it is not possible to constrain this exponent any better, and it is best to obtain further constraints on the value of this exponent from models of point defects, as done in Part II.
4. Below oxygen fugacities of 10^{-10} Pa at lower temperatures (below $\sim 950^\circ\text{C}$), the oxygen fugacity dependence of diffusion rates diminishes to the point of practically vanishing. The activation energy of diffusion obtained by fitting data in this region (e.g. $fO_2 = 10^{-12}$ Pa) is slightly higher, 223 ± 9 kJ/mol. In combination, these document a change of diffusion mechanism in olivine that is further quantified in Part II.
5. Our expanded database on Fe–Mg diffusion over a range of temperature and fO_2 confirm the observations of Petry et al. (2004), made on the basis of comparisons with the relatively limited dataset of Chakraborty (1997), that diffusion rates of other divalent cations, such as Mn and Ni, are practically identical to those of Fe–Mg diffusion. Ni diffusion may be slightly slower

on the average. On the other hand, Ca diffusion rates (Coogan et al. 2005) are substantially slower (by a factor of about 10 along [001]) than rates of Fe–Mg diffusion.

The most important implication of this data set is that with the availability of diffusion coefficients determined experimentally down to temperatures of 700°C , and a wide range of composition, fO_2 and crystallographic orientation, most modeling of natural samples can be carried out by *interpolating*, rather than *extrapolating*, laboratory data for the first time. After considering a mechanistic interpretation of this data and change of mechanism based on point defect chemistry, we provide master equations to calculate Fe–Mg diffusion coefficients in olivine for modeling any natural process in Part II.

Acknowledgments Undergraduate students Julia Halfmann and Daniela Lüttgebüter have provided substantial help in the high temperature furnace laboratory as well as in the thin film deposition laboratory at different stages of this work. In addition, Julia Halfmann helped with white light interference microscopy. Their enthusiasm was contagious. The help of Dr. Rolf Neuser at the SEM and Dr. Hans-Jürgen Bernhardt at the microprobe laboratory were indispensable. Dr. W. Gebert oriented some of the olivine crystals for us. None of the experiments would be possible without the efforts of Tanya Westphal at the polishing lab. The German Science Foundation (DFG) generously sustained this project through material support and by covering the entire salary of the first author. This support was obtained in part within the interdisciplinary program SFB 526 (Rheology of the Earth). We gratefully acknowledge the help from all of these individuals and organizations. Finally, we thank Daniele Cherniak and Bill Carlson for their constructive reviews which helped to revise the manuscript.

References

- Bai Q, Kohlstedt DL (1993) Effects of chemical environment on the solubility and incorporation mechanism for hydrogen in olivine. *Phys Chem Miner* 19:460–471
- Barkmann T, Cemic L (1996) Impedance spectroscopy and defect chemistry of fayalite. *Phys Chem Miner* 23:186–192
- Buening DK, Buseck PR (1973) Fe–Mg lattice diffusion in olivine. *J Geophys Res* 78:6852–6862
- Chakraborty S (1997) Rates and mechanisms of Fe–Mg interdiffusion in olivine at 980°C – 1300°C . *J Geophys Res* 102(B6):12317–12331
- Chakraborty S, Costa F (2004) Fast diffusion of Si and O in San Carlos olivine under hydrous conditions. *Geochim Cosmochim Acta* 68(Suppl. S):A275
- Chakraborty S, Ganguly J (1992) Cation diffusion in aluminosilicate garnets: experimental determination in spessartine–almandine diffusion couples, evaluation of effective binary diffusion coefficients, and applications. *Contrib Mineral Petrol* 111:74–86
- Chakraborty S, Farver JR, Yund RA, Rubie DC (1994) Mg tracer diffusion in synthetic forsterite and San Carlos olivine as a function of P , T , and fO_2 . *Phys Chem Miner* 21:489–500
- Cherniak DJ, Lanford WA, Ryerson FJ (1991) Lead diffusion in apatite and zircon using ion implantation and Rutherford Backscattering techniques. *Geochim Cosmochim Acta* 55:1663–1673

- Chrisey DB, Hubler GK (eds) (1994) Pulsed laser deposition of thin films. Wiley, New York, pp 613
- Clark AM, Long JVP (1971) The anisotropic diffusion of nickel in olivine. In: Sherwood JN, Chadwick AV, Muir WM, Swinton FL (eds) Diffusion processes. Gordon and Breach, London, pp 511–521
- Coogan L, Hain A, Stahl S, Chakraborty S (2005) Experimental determination of the diffusion coefficient for calcium in olivine between 900°C and 1500°C. *Geochim Cosmochim Acta* 69:3683–3694
- Costa F, Chakraborty S (2004) Decadal time gaps between mafic intrusion and silicic eruption obtained from chemical zoning patterns in olivine. *Earth Planet Sci Lett* 227:517–530
- Costa F, Dungan M (2005) Short time scales of magmatic assimilation from diffusion modeling of multiple elements in olivine. *Geology* 33:837–840
- Crank J (1975) *The Mathematics of Diffusion*. Oxford University Press, New York, pp 414
- Dohmen R, Becker H-W, Meissner E, Etzel T, Chakraborty S (2002) Production of silicate thin films using pulsed laser deposition (PLD) and applications to studies in mineral kinetics. *Eur J Mineral* 14:1155–1168
- Dohmen R, Chakraborty S, Palme H, Rammensee W (2003) The role of element solubility on the kinetics of element partitioning: in situ observations and a thermodynamic kinetic model. *J Geophys Res* 108(B3):2157. doi:10.1029/2001JB000587
- Doolittle LR (1986) A semiautomatic algorithm for Rutherford backscattering spectra. *Nucl Instrum Methods B* 15:227–231
- Düffels K, Chakraborty S, Brenker F (2004) Enhancement of diffusion rates in olivine during evaporation—an example of reactive diffusion in a mineralogical system. *Lithos* 73(Suppl. S):S30
- Farver JR, Yund RA, Rubie DC (1994) Magnesium grain boundary diffusion in forsterite aggregates at 1000°C–1300°C and 0.1 MPa to 10 GPa. *J Geophys Res* 99:19809–19819
- Feldman LC (1986) *Fundamentals of surface and thin film analysis*. North-Holland, New York, pp 352
- Ganguly J, Bhattacharya RN, Chakraborty S (1988) Convolution effects in the determination of compositional profiles and diffusion coefficients by microprobe step scan. *Am Mineral* 73:901–909
- Ganguly J, Chakraborty S, Sharp TG, Rumble III D (1996) Constraint on the time scale of biotite-grade metamorphism during Acadian orogeny from a natural garnet–garnet diffusion couple. *Am Miner* 81:1208–1216
- Harrison LG (1961) Influence of dislocations on diffusion kinetics in solids with particular reference to alkali halides. *Trans Faraday Soc* 57:1191–1199
- Hermeling J, Schmalzried H (1984) Tracerdiffusion of the Fe-cations in Olivine ($\text{Fe}_x\text{Mg}_{1-x}$)₂SiO₄ (III). *Phys Chem Miner* 11:161–166
- Hier-Majumder S, Anderson IM, Kohlstedt DL (2005) Influence of protons on Fe–Mg interdiffusion in olivine. *J Geophys Res* 110:B02202. doi: 10.1029/2004JB003292
- Ito M, Yurimoto M, Morioka M, Nagasawa H (1999) Co²⁺ and Ni²⁺ diffusion in olivine determined by secondary ion mass spectrometry. *Phys Chem Miner* 26:425–431
- Jaoul O, Sautter V, Abel F (1991) Nuclear microanalysis: a powerful tool for measuring low atomic diffusivity with mineralogical applications, in diffusion, atomic ordering, and mass transport. *Sel Top Geochem* 8:198–220
- Jaoul O, Bertran-Alvarez Y, Liebermann RC, Price DP (1995) Fe–Mg interdiffusion in olivine up to 9 GPa at $T = 600$ – 900°C ; experimental data and comparison with defect calculations. *Phys Earth Planet Inter* 89:199–218
- Jurewicz AJG, Watson EB (1988) Cation in olivine, Part 1: calcium partitioning and calcium–magnesium distribution between olivines and coexisting melts, with petrologic applications. *Contrib Mineral Petrol* 99:176–185
- Kotai E (1994) Computational methods for analysis and simulation of RBS and ERDA spectra. *Nucl Instr Meth B* 85:588–596
- Lovering TS (1936) Heat conduction in dissimilar rocks and the use of thermal models. *Bull Geol Soc Am* 47:87–100
- Meissner E, Sharp TG, Chakraborty S (1998) Quantitative measurement of short compositional profiles using analytical transmission electron microscopy. *Am Miner* 83:546–552
- Misener DJ (1974) Cation diffusion in olivine to 1400°C and 35 kbar. In: Hofmann AW, Giletti BJ, Yoder HS Jr, Yund RA (eds) *Geochemical transport and kinetics*. Carnegie Inst. Wash. Publ., vol 634. Washington Carnegie Inst., pp 117–129
- Morioka M (1981) Cation diffusion in olivine—II. Ni–Mg, Mn–Mg, Mg and Ca. *Geochim Cosmochim Acta* 45:1573–1580
- Morioka M, Nagasawa H (1991) Ionic diffusion in olivine. In: Ganguly J (ed) *Diffusion, atomic ordering and mass transport*. *Adv Phys Geochem* 8:176–197. Springer, Heidelberg
- Nakamura A, Schmalzried H (1983) On the nonstoichiometry and point defects of olivine. *Phys Chem Miner* 10:27–37
- Nakamura A, Schmalzried H (1984) On the Fe²⁺–Mg²⁺-interdiffusion in olivine (II). *Ber Bunsenges Phys Chem* 88:140–145
- Petry C, Chakraborty S, Palme H (2004) Experimental determination of Ni diffusion coefficients in olivine and their dependence on temperature, composition, oxygen fugacity, and crystallographic orientation. *Geochimica Cosmochimica Acta* 68:4179–4188
- Rumble III D, Finnerty TA (1974) Devonian Grossularite–Spessartine overgrowths on Ordovician Almandine from Eastern Vermont. *Am Miner* 59:558–562
- Schmalzried H (1981) *Solid state reactions*. Verlag Chemie, Weinheim
- Stocker RL, Smyth DM (1978) Effect of enstatite activity and oxygen partial pressure on the point defect chemistry of olivine. *Phys Earth Planet Inter* 16:145–156
- Tirone M, Ganguly J, Dohmen R, Langenhorst F, Hervig R, Becker H-W (2005) Rare earth diffusion kinetics in garnet: experimental studies and applications. *Geochim Cosmochim Acta* 69:2385–2398
- Tsai T-L, Dieckmann R (2002) Variation of the oxygen content and point defects in olivines, $(\text{Fe}_x\text{Mg}_{1-x})_2\text{SiO}_4$, $0.2 \leq x \leq 1.0$. *Phys Chem Miner* 29:680–694